https://doi.org/10.5194/amt-2020-466
Preprint. Discussion started: 22 December 2020

Atmospheric Measurement Techniques Discussions

Retrieval Algorithm for the Column CO_2 Mixing Ratio from Pulsed Multi-Wavelength Lidar Measurements

Xiaoli Sun[1], James B. Abshire[1,2], Anand Ramanathan[3], S. Randy Kawa[1], and Jianping Mao[2]

[1]NASA Goddard Space Flight Center, Code 698/690/614, Greenbelt, Maryland, USA
[2]University of Maryland, College Park, Maryland, USA
[3]Audible, Inc., Newark, New Jersey, USA

Correspondence to: Xiaoli Sun (xiaoli.sun-1@nasa.gov)

Abstract. The retrieval algorithm for the column mixing ratio of CO_2 from the measurements of a pulsed multi-wavelength integrated path differential absorption (IPDA) lidar is described. The lidar samples the shape of the 1572.33 nm CO_2 absorption line at 15 or 30 wavelengths. The algorithm uses a least-squares fit between the CO_2 line shape computed from a layered atmosphere model to that sampled by the lidar. In addition to the column average CO_2 dry air mole fraction (XCO_2), several other parameters are also solved simultaneously from the fit. These include the Doppler shift in the received laser signal wavelengths, the product of the surface reflectivity and atmospheric transmission and a linear trend in the lidar receiver's spectral response. The algorithm can also be used to solve for the average water vapor mixing ratio, which causes a secondary absorption in the wings of the CO_2 absorption line under high humidity conditions. The least-squares fit is linearized about the expected XCO_2 value which allows the use of a standard linear least-squares fitting method and software tools. The standard deviation of the retrieved XCO_2 is obtained from covariance matrix of the fit. An averaging kernel is defined similarly to that used for passive trace-gas sounding. Examples are presented of using the algorithm to retrieve XCO_2 from the measurements from NASA Goddard's airborne CO_2 Sounder lidar made at a constant altitude and during spiral-down maneuvers.

1 Introduction

Accurate remote sensing of atmospheric CO_2 from Earth orbiting satellites is a key component in the long-term carbon–climate observing system (Sellers et al., 2018). Airborne and spaceborne lidar can be used to remotely monitor the global CO_2 and other trace-gas concentrations under conditions that are inaccessible to passive space-borne CO_2 measurement missions, such as GOSAT (Kuze et al., 2016), OCO-2 (Crisp, 2017), and OCO-3 (Eldering et al., 2017; 2019). Studies have shown (Kawa et al., 2018) that a polar orbiting integrated path differential absorption (IPDA) lidar can measure XCO_2 with low bias and high precision at all sun angles, seasons and latitudes using a constant nadir-zenith illumination and observing geometry. A pulsed IPDA lidar provides the range-resolved atmospheric backscatter profiles, so that return signals from the surface, clouds, and aerosols can be uniquely separated. This allows pulsed IPDA lidar to measure XCO_2 to the surface, cloud tops, or both (Ramanathan et al., 2015). Because the laser pulses reflected from clouds, aerosols and surface are separated in time, the XCO_2 retrievals to the ground surface are not affected by multiple scattering from clouds and aerosols (Mao et al., 2018).

https://doi.org/10.5194/amt-2020-466
Preprint. Discussion started: 22 December 2020


Atmospheric Measurement Techniques Discussions

Several types of on-line and off-line dual wavelength IPDA lidar have been demonstrated previously for measuring XCO_2 from aircraft (Spiers et al., 2011; Menzies et al., 2014; Jacob et al., 2019; Dobler et al., 2013; Refaat et al., 2016, 2020; and Amediek et al., 2017). A multi-wavelength IPDA lidar has also been reported (Zhu et al., 2019, 2020). The retrieval algorithms used in these IPDA lidar calculate the ratios of on-line to the off-line atmosphere transmission, convert them to differential absorption optical depths (DAOD), and then solve for XCO_2 from the DAOD based on the atmosphere models. In the case of a multi-wavelength lidar, a series of DAODs are calculated and a least-squares fit is used to solve for XCO_2 (Han et al., 2020).

NASA Goddard Space Flight Center (GSFC) had previously developed an airborne multi-wavelength CO_2 Sounder lidar and demonstrated XCO_2 measurements through a series of airborne campaigns (Abshire et al., 2010, 2013, 2014, 2018; Ramanathan et al., 2013, 2015, 2018; Mao et al., 2018). The retrieval algorithm uses for the lidar was largely based on the approach used for passive trace gas measurements with modifications specifically for the lidar measurement. The retrieval algorithm compares the lidar-sampled line shape with the one computed from an atmosphere model. The XCO_2 and several other parameters are solved via a least-squares fit.

This paper describes the retrieval algorithm for the multi-wavelength CO_2 Sounder lidar and provides a framework for similar IPDA lidar for other atmospheric gas measurements. Parts of the algorithm have been reported earlier (Ramanathan et al., 2013, 2015, 2018). This paper gives a complete description of the algorithm, the mathematical derivations, signal processing techniques, estimation error, and averaging kernel. An example of the use of the algorithm with the airborne CO_2 Sounder lidar measurement data is also presented.

2. Measurement Approach

The measurement geometry for the CO_2 Sounder lidar is shown in Fig. 1. The lidar transmits laser pulses toward nadir and its receiver telescope collects the optical signal backscattered from the atmosphere and the surface. The receiver detects and records the received laser pulse waveform over the entire atmosphere column traveled by the laser pulses. The received signal from the surface are used to retrieve XCO_2. The signals before the ground returns are used to obtain the atmosphere backscatter profiles as an ancillary data set. The signals recorded after the ground returns are used to estimate the solar background, the detector dark noise, and the baseline voltage offset in the detector output. The baseline offset is subtracted from the signal before calculating the ground return pulse energies. The times-of-flight of the laser pulse are used to determine the atmosphere column height for the CO_2 is measured. Figure 2 shows a block diagram of the airborne CO_2 Sounder lidar developed at NASA GSFC. It was developed as an airborne demonstrator for the Active Sensing of CO_2 Emission over Days, Nights, and Seasons (ASCENDS) mission (Kawa et al., 2018).

The laser consists of a tunable seed laser, a pulsed modulator and a power amplifier. The seeder laser module consists of two single-frequency continuous wave (CW) diode lasers. One is the master with its wavelength locked to the center of the CO_2 absorption line. The other one is the slave with its wavelength locked to that of the master plus an offset frequency. The

https://doi.org/10.5194/amt-2020-466
Preprint. Discussion started: 22 December 2020

Atmospheric Measurement Techniques Discussions

offset frequency is step-tuned between laser pulses to scan across the CO_2 absorption line. The number of laser wavelengths in the scan and the exact wavelength of each laser pulse are preprogrammed and can be adjusted via software commands (Numata et al., 2012). An electro-optical modulator is used to gate the output of the slave laser into 1-μsec wide pulses. The laser pulses are then amplified by a multi-stage fiber laser amplifier. The airborne lidar's laser pulse rate is 10 KHz and there are 30 wavelengths per scan, which gives a wavelength scan rate of about 300 Hz. The transmitted laser pulse energies at all wavelengths are also sampled and the results are used to normalize the received signal to correct for the effects of laser power fluctuations.

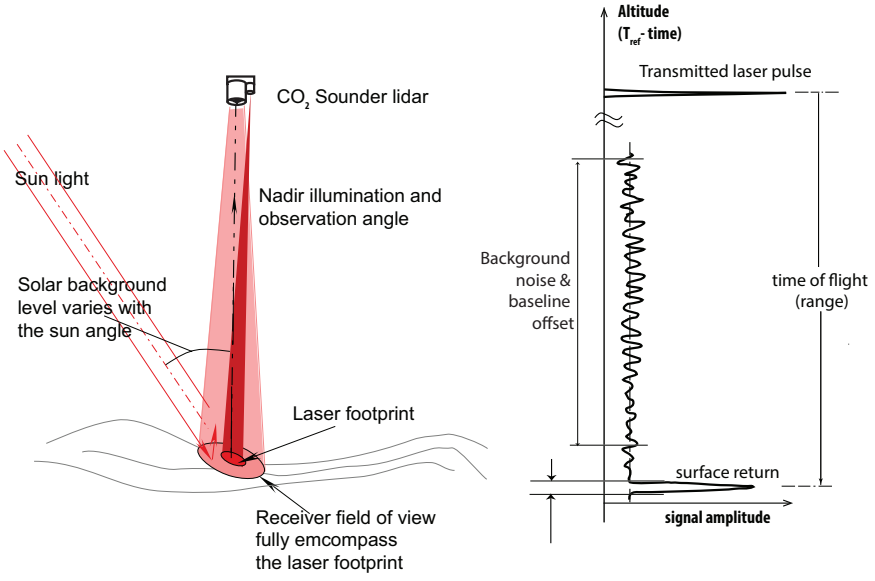

Figure 1. Illustrations of the CO_2 Sounder lidar measurement geometry and received signal at a single laser wavelength.

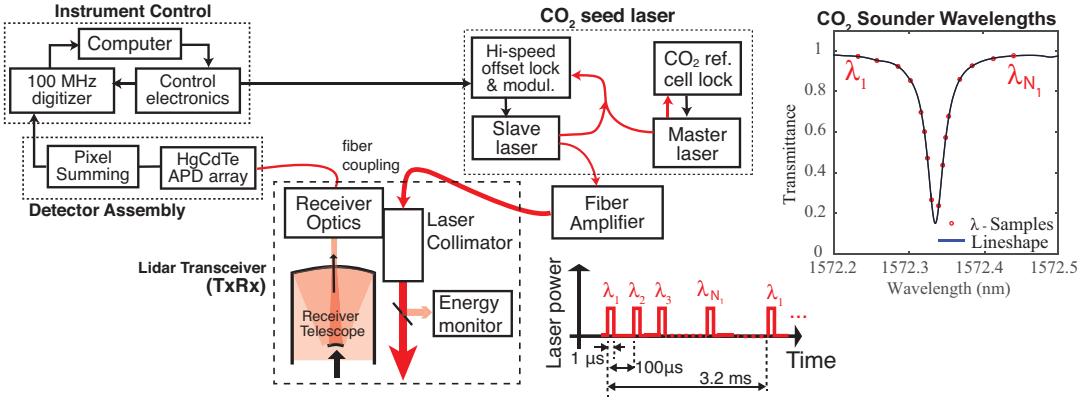

Figure 2. Block diagram of the airborne CO_2 Sounder lidar developed at NASA GSFC.

https://doi.org/10.5194/amt-2020-466
Preprint. Discussion started: 22 December 2020

Atmospheric Measurement Techniques Discussions

3. Lidar Signal Processing and Atmosphere Modeling

The initial processing of the lidar data consists of (a) processing the stored lidar data to form a series of atmosphere transmission measurements across the CO_2 absorption line; (b) generating a CO_2 absorption line shape from the radiative transfer model and mereological data at the time and location of lidar measurements; and (c) performing a least-squares fit of the modeled line shape function to the measurements to solve for XCO_2, as shown in Fig. 3.

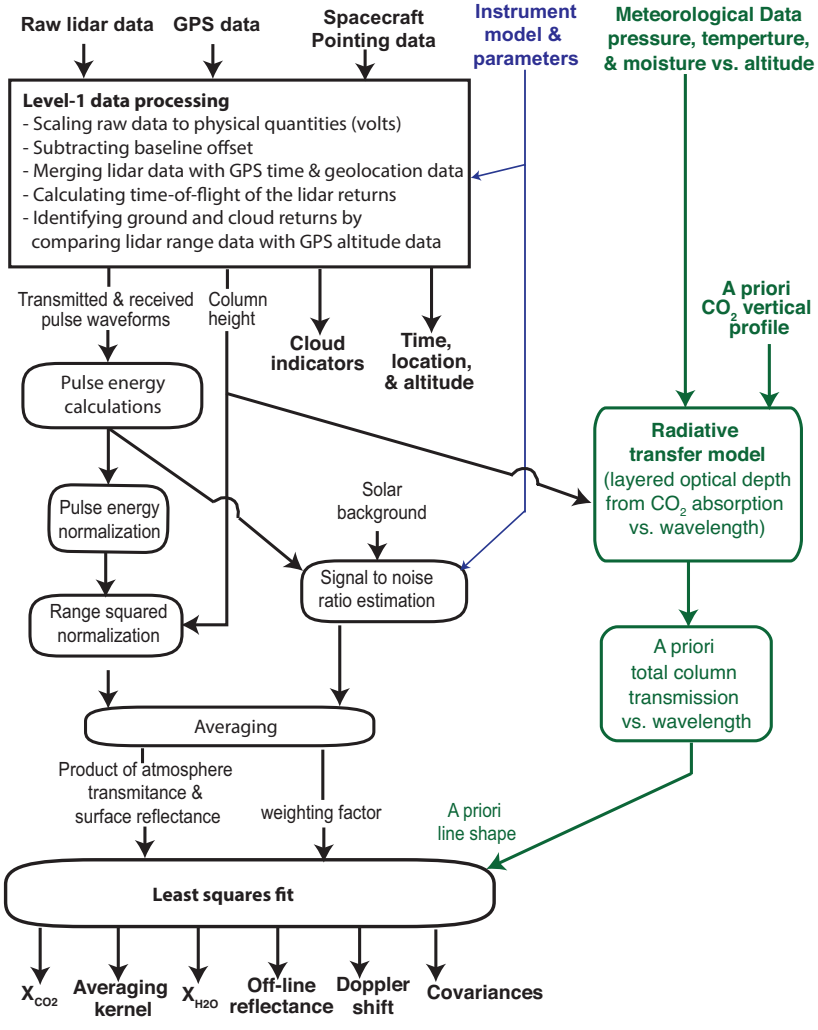

Figure 3. Flowchart of the XCO_2 retrieval algorithm for the CO_2 Sounder lidar.

https://doi.org/10.5194/amt-2020-466
Preprint. Discussion started: 22 December 2020


Atmospheric Measurement Techniques Discussions

3.1. Lidar Signal Processing

The signal waveforms are first corrected for the detector baseline offset and other instrument characteristics and then scaled to the received optical signal power. The pulse energies from the scattering surfaces are calculated by integrating the received pulse waveforms over the pulse width interval. The relative atmosphere transmittances for all laser wavelengths are calculated by dividing the received pulse energies by the transmitted ones and then multiplying by the square of the range from the lidar to the reflecting surface. The signal to noise ratio (SNR) of the atmospheric transmittances at each wavelength is estimated based on the received signal energy, the estimated background noise, and the inherent instrument noise. Finally, a least-squares fit of the modeled line shape to the lidar measurements is used to estimate XCO_2 along with the other parameters.

The lidar returns from clouds are identified by comparing the target elevation from the lidar measurements, namely, aircraft altitude minus the lidar range, to the surface elevation from either the on-board radar measurements or from a Digital Elevation model (DEM). For dense clouds, the signal pulse energies from the clouds are sufficient for XCO_2 retrieval to the cloud top (Mao et al., 2018). For thin clouds and aerosols, the laser pulses can often reach the ground surface and with sufficient SNR for XCO_2 retrievals to the surface. The signal waveform prior to the ground return can be averaged to obtain the atmospheric backscatter profiles at the laser wavelength which gives information about the height and density of the clouds and aerosols (Allan et al., 2019).

3.2. Model for the Lidar Signals

The average signal pulse energy reflected from the surface can be calculated from the lidar equation (McManamon, 2019), as

$$E_r(\lambda) = E_t(\lambda) \cdot T_A^2(\lambda) \frac{r_s}{\pi} \cdot \frac{A_r}{R^2} \cdot \eta_r \quad (1)$$

where

$E_r(\lambda)$ and $E_t(\lambda)$ are the received and transmitted laser pulse energies;

λ is the laser wavelength;

$T_A(\lambda)$ is the one-way atmosphere transmission as a function of the laser wavelength;

r_s is the diffuse surface reflectance in nadir direction;

A_r is the collecting area of the receiver telescope;

R is the range from the lidar to the scattering surface (the column height);

η_r is the receiver optical transmission efficiency.

The product of the surface reflectance and the two-way atmospheric transmission can be calculated from the received laser pulse energy after correcting for the range, as

$$y(\lambda) = r_s T_A^2(\lambda) = c_1 \frac{E_r(\lambda)}{E_t(\lambda)} \cdot \frac{1}{R^2}. \quad (2)$$

Here c_1 is a constant which is a function of the lidar instrument parameters and can be calibrated independently.

https://doi.org/10.5194/amt-2020-466
Preprint. Discussion started: 22 December 2020


Atmospheric Measurement Techniques Discussions

3.3. Model for the CO_2 Absorption Line Shape

The total atmospheric transmission to the surface can be written as

$$T_A^2(\lambda) = T_{CO2}^2(\lambda) \cdot T_w^2(\lambda) \cdot T_o^2. \quad (3)$$

The first two terms, $T_{CO2}^2(\lambda)$ and $T_w^2(\lambda)$ are the two-way transmissions due to CO_2 and water vapor which are functions of the laser wavelength λ. The last term, T_o^2, accounts for the transmission of aerosols and other particles, which are independent of the laser wavelength. T_o^2 is often called the off-line atmospheric transmission.

To model the total atmosphere transmissions due to CO_2 and water vapor, the atmosphere is divided into a number of layers. The total transmission is modeled as the product of the transmissions of all the layers traveled by the laser pulse. The layered transmission is calculated from the layered radiative transfer atmospheric model, which takes into account of the effects of the temperature, pressure, and humidity at the altitude of the layer. The vertical profiles of temperature, pressure and humidity are obtained from a meteorological analysis model or from other atmospheric data along with an *a priori* vertical profile of CO_2 mixing ratios.

The atmospheric transmissions of each layer for each of the lidar wavelength across the CO_2 absorption line are calculated using the Beer-Lambert law. The total two-way transmission due to CO_2 can be written as

$$T_{CO2}^2(\lambda_i) = exp\left[-2\sum_{j=1}^{N_2} \rho_{CO2}(H_j)\sigma_{CO2}(H_j, \lambda_i)\,\Delta H_j\right] \quad (4)$$

where

$i = 1,2,\ldots,N_1$ is the index for the laser wavelengths with N_1 the total number of laser wavelengths used in the lidar measurements;

$j = 1,2,\ldots,N_2$ is the index for the atmosphere layer with N_2 the total number atmosphere layers;

$\rho_{CO2}(H_j)$ is the CO_2 molecular density for the jth layer;

H_j is the average altitude of the jth layer;

$\sigma_{CO2}(H_j, \lambda_i)$ is the absorption cross-section of a CO_2 molecule in the jth layer at the ith wavelength.

The CO_2 molecular density for the jth layer can be expressed as

$$\rho_{CO2}(H_j) = xco2_j\ \rho_{air}(H_j), \quad (5)$$

with $xco2_j$ the CO_2 mixing ratio and $\rho_{air}(H_j)$ the dry air molecular density at altitude H_j.

For each laser wavelength the optical transmissions of CO_2 for each layer are calculated from their optical depth (OD), which is defined as the absolute value of the logarithm of the one-way atmospheric transmission. The total column OD is then calculated by summing the layered ODs over the column height of the lidar measurement. The two-way optical transmission is given by $T_{CO2}^2(\lambda_i) = exp[-2\mathrm{OD}(\lambda_i)]$. In our XCO_2 retrieval the layered OD is calculated by using the spectroscopy database HITRAN 2008 (Rothman et al., 2009) and the Line-By-Line Radiative Transfer Model (LBLRTM)

https://doi.org/10.5194/amt-2020-466
Preprint. Discussion started: 22 December 2020


Atmospheric Measurement Techniques Discussions

V12.1, (Clough et al., 1992; Clough and Iacono, 1995), for the *a priori* CO_2 mixing ratio and meteorological vertical profiles at the time and location of the lidar measurement.

The atmospheric pressure, temperature and water vapor profiles influence line broadening which affects the cross section of the CO_2 molecule. The LBLRTM software incorporates these effects and computes a numerical line shape function in OD at the given altitude of each layer. For the airborne data retrievals, meteorological data are obtained from the near real-time forward processing of the Goddard Modeling and Assimilation Office, (GMAO) FP system, the Goddard Earth Observing System Model, Version 5 (GEOS-5) (Rienecker et al., 2008). The data are drawn from the 8-per-day analyzed fields on the full model grid (0.25 x 0.3125 deg x 72 layers, inst3_3d_asm_Nv files). The GEOS-5 data are used for the meteorological conditions for the retrievals for the times and places where the mission-directed atmospheric measurements are not available. In measurement campaigns this occurred for most of the flights except for those in spiral maneuvers. We extract the nearest-in-time, latitude-longitude interpolated meteorological soundings every minute at regular positions along the flight's ground tracks. The 42 lowest analysis levels are used for each profile location. Analyzed pressure is used for the vertical grid coordinate for any of the profiles. The surface pressure and surface height are horizontally interpolated from the model.

Ideally, we would want to retrieve the CO_2 mixing ratio at each layer, as in conventional passive trace gas sounding. In practice, the average laser power is limited and there can only be a limited number of laser wavelength samples across the CO_2 absorption line while still maintaining adequate SNR at each wavelength. Although a few more parameters about the CO_2 absorption line shape can be retrieved (Ramanathan et al., 2018), they are not sufficient to provide the full vertical profile of CO_2 mixing ratio. Therefore, we choose to solve for a scale factor for the modeled CO_2 line shape function that minimizes the error between the modeled and the lidar sampled CO_2 absorption line shape at all laser wavelengths. The retrieved average XCO_2 is equal to the product of this scale factor and the *a priori* CO_2 mixing ratio. This method has been shown to work well in simulations and for retrievals from our airborne CO_2 Sounder lidar measurements (Kawa et al., 2016; Abshire et al., 2014, 2018).

Using the scale factor, the OD which is attributable to the CO_2 absorption can be written as

$$OD_{CO2}(\lambda_i) \approx \alpha_{CO2} \sum_{j=1}^{N_2} \overline{xco2}_j \, \rho_{air}(H_j) \, \sigma_{CO2}(H_j, \lambda_i) \, \Delta H_j = \alpha_{CO2} \overline{OD}_{CO2}(\lambda_i) \quad (6)$$

where α_{CO2} is the scale factor, $\overline{xco2}_j$ is the *a priori* CO_2 mixing ratio, and $\overline{OD}_{CO2}(\lambda_i)$ is the *a priori* OD attributed to CO_2 absorption. The atmospheric transmission due to CO_2 absorption can now be approximated as

$$T^2_{CO2}(\lambda_i) \approx exp\{-2 \, \alpha_{CO2} \overline{OD}_{CO2}(\lambda_i)\}. \quad (7)$$

4. Solving for XCO_2 from the Lidar Measurements via a Least-Squares Fit

The column XCO_2 and several other variables are solved simultaneously from a least-squares fit of the modeled line shape to the lidar measurements. One of them is the Doppler shift in the wavelengths of the received signal, which occurs when measuring at non-nadir angles or to a sloped surface. Another parameter being solved is the product of the surface reflectance and the two-way off-line atmospheric transmission. For the CO_2 line at 1572.33 nm and under high humidity, there is a weak

https://doi.org/10.5194/amt-2020-466
Preprint. Discussion started: 22 December 2020


Atmospheric Measurement Techniques Discussions

water vapor absorption feature on the left wing of the CO_2 absorption line. The retrieval algorithm can solve this absorption feature to avoid compensating it and causing biases in the retrieved XCO_2. For our airborne lidar, there is a small linear trend (slope) in the received laser pulse energy as a function of the wavelength. A likely cause of this trend is the residual errors from correction of the uneven receiver spectral response of the optics, especially the optical bandpass filter. Since this is known to drift over temperature and time, the retrieval solves for this residual slop for every point of the XCO_2 retrieval.

The least-squares fit may be formulated by expressing the lidar measurement data in matrix form, $\boldsymbol{Y}$, a single column matrix with elements y_i given by Eq. (2). The parameters to be solved, $\boldsymbol{S} = \{s_k\}$, is expressed as a $N_3 \times 1$ matrix. In our case $N_3 = 5$, and each element is defined as

$s_1 = r_s T_o^2$ is the product of the surface reflectance and the two-way atmosphere transmission at off-line wavelength;

$s_2 = \alpha_{CO2}$ is the scale factor for the XCO_2 line shape function;

$s_3 = \alpha_{water}$ is the scale factor for the water vapor line shape function;

s_4 is the linear slope of the receiver spectral response.

s_5 is the Doppler shift of the received signal wavelength.

The modeled atmospheric transmission given in Eq. (7) can be expressed as a single column matrix, $\boldsymbol{F}(\boldsymbol{S})$, with each element equal to

$$f_i(\boldsymbol{S}) = r_s T_A^2(\lambda_i, \boldsymbol{S}) \approx s_1[s_2 T_{co2}^2(\lambda_i + s_5)][s_3 T_{water}^2(\lambda_i + s_5)]\eta_0(\lambda_i + s_5, s_4) \quad (8)$$

where $T_A^2(\lambda, \boldsymbol{S})$ is the atmosphere transmission defined in Eq. (1) but expressed as a function of both the laser wavelength and the parameters to be solved, and $\eta_0(\lambda, s_4)$ is the normalized receiver optical transmission as a function of the wavelength and the slope of the linear trend of the receiver spectral response. Here we also included the term for the water vapor.

A scalar-valued loss function can be defined as the sum of squared differences between the lidar measurement data and the model, as,

$$J(\boldsymbol{Y}, \boldsymbol{S}) = [\boldsymbol{Y} - \boldsymbol{F}(\boldsymbol{S})]^T \boldsymbol{W} [\boldsymbol{Y} - \boldsymbol{F}(\boldsymbol{S})] = \sum_{i=1}^{N_1} w_{i,i}[y(\lambda_i) - f_i(\boldsymbol{S})]^2 \quad (9)$$

where $[\boldsymbol{Y} - \boldsymbol{F}(\boldsymbol{S})]$ is an $N_1 \times 1$ matrix and $\boldsymbol{W}$ is a $N_1 \times N_1$ diagonal matrix for the weighting factors. The weighting factors are chosen to balance out the contributions from the measurements at different laser wavelengths with different SNRs. The least-squares fit finds the parameter set that minimizes the loss function.

For small changes in XCO_2 and high SNR lidar measurements, Eq. (9) can be "linearized" by the first two terms of its power series expansion about initial estimates of the parameter values, $\boldsymbol{S0}$. The function $\boldsymbol{F}(\boldsymbol{S})$, which sometimes is called forward model, can then be approximated by

$$\boldsymbol{F}(\boldsymbol{S}) \approx \boldsymbol{F0} + \frac{\partial \boldsymbol{F}(\boldsymbol{S})}{\partial \boldsymbol{S}}\Big|_{\boldsymbol{S}=\boldsymbol{S0}} (\boldsymbol{S} - \boldsymbol{S0}) \quad (10)$$

where

$$\boldsymbol{F0} = \boldsymbol{F}(\boldsymbol{S0}) = \begin{bmatrix} f0(\lambda_1) \\ \vdots \\ f0(\lambda_{N_1}) \end{bmatrix}$$

https://doi.org/10.5194/amt-2020-466
Preprint. Discussion started: 22 December 2020


Atmospheric Measurement Techniques Discussions

with $f0(\lambda_i)$ equal to Eq. (8) evaluated at the initial value of the parameter set.

Substituting Eq. (10) into Eq. (9) and defining $\boldsymbol{\Delta Y} = (\boldsymbol{Y} - \boldsymbol{F0})$ and $\boldsymbol{\Delta S} = \boldsymbol{S} - \boldsymbol{S0}$, the loss function can now be approximated as

$$J(\boldsymbol{Y},\boldsymbol{S}) \approx \left[\boldsymbol{\Delta Y} - \frac{\partial \boldsymbol{F(S)}}{\partial \boldsymbol{S}}|_{\boldsymbol{S=S0}}\,\boldsymbol{\Delta S}\right]^T \boldsymbol{W}\left[\boldsymbol{\Delta Y} - \frac{\partial \boldsymbol{F(S)}}{\partial \boldsymbol{S}}|_{\boldsymbol{S=S0}}\,\boldsymbol{\Delta S}\right]. \quad (11)$$

For mathematical convenience, we normalize the lidar measurements with respective to their initial estimate and define a new variable

$$\Delta y1(\lambda_{i1}) = \frac{\Delta y(\lambda_i)}{f0(\lambda_i)}. \quad (12)$$

A diagonal matrix $\boldsymbol{I_O}$ can be defined with each element equal to $1/f0(\lambda_i)$. The loss function can be rewritten using the identity matrix $\boldsymbol{I} \equiv \boldsymbol{I_O}\,\boldsymbol{I_O}^{-1} \equiv \boldsymbol{I_O}^{-1}\boldsymbol{I_O}$, as,

$$\begin{aligned} J(\boldsymbol{Y},\boldsymbol{S}) &\approx \left[\boldsymbol{\Delta Y} - \frac{\partial \boldsymbol{F(S)}}{\partial \boldsymbol{S}}|_{\boldsymbol{S=S0}}\boldsymbol{\Delta S}\right]^T (\boldsymbol{I_O}\,\boldsymbol{I_O}^{-1})\boldsymbol{W}(\,\boldsymbol{I_O}^{-1}\boldsymbol{I_O})\left[\boldsymbol{\Delta Y} - \frac{\partial \boldsymbol{F(S)}}{\partial \boldsymbol{S}}|_{\boldsymbol{S=S0}}\boldsymbol{\Delta S}\right] \\ &= \left[\boldsymbol{\Delta Y1} - \frac{\partial \boldsymbol{F1(S)}}{\partial \boldsymbol{S}}\,\boldsymbol{\Delta S}\right]^T \boldsymbol{W1}\,\left[\boldsymbol{\Delta Y1} - \frac{\partial \boldsymbol{F1(S)}}{\partial \boldsymbol{S}}\,\boldsymbol{\Delta S}\right] \end{aligned} \quad (13)$$

where $\boldsymbol{\Delta Y1} = \boldsymbol{I_O}\boldsymbol{\Delta Y}$, $\boldsymbol{F1(S)} = \boldsymbol{I_O}\boldsymbol{F(S)}$, and $\boldsymbol{W1} = \boldsymbol{I_O}^{-1}\boldsymbol{W}\boldsymbol{I_O}$.

The loss function given in Eq. (13) is of the same form as that of a linear least-squares fit with measurement data $\boldsymbol{\Delta Y1}$ and weighting factor $\boldsymbol{W1}$. The derivative of the function $\boldsymbol{F(S)}$, which is often referred to as the Jacobian, is given by

$$\boldsymbol{K} = \frac{\partial[\boldsymbol{F1(S)}\,]}{\partial \boldsymbol{S}}|_{\boldsymbol{S=S0}}. \quad (14)$$

For the CO_2 Sounder lidar, each term of the Jacobian can be derived as

$k_{i,1} = \frac{\partial \boldsymbol{F(S)}}{s_1}\frac{1}{f0(\lambda_i)} = \frac{1}{\langle r_s T_o^2\rangle}$, same for all $i = 1,2,\ldots N_1$;

$k_{i,2} = -2\overline{OD}_{CO2}(\lambda_i)$, one for each laser wavelength, $i = 1,2,\ldots N_1$;

$k_{i,3}$, same as above but for water vapor;

$k_{i,4} \approx \frac{T_{CO2}^2(\lambda_i+\Delta\lambda) - T_{CO2}^2(\lambda_i)}{\Delta\lambda} \cdot \frac{1}{\langle T_{CO2}^2(\lambda_i)\rangle}$, which can be obtained from the modeled line shape function;

$k_{i,5} = (\lambda_i - \lambda_c)$, with λ_c the center wavelength of the CO_2 line shape function.

For measurement noise that is zero-mean and follows a Gaussian distribution, the optimal weighting factors are given by the reciprocal of the variance of the measurement data (Bevington 1969). In our case, the optimal weighting factors can be approximated as

$$w1_{i,i} = \frac{1}{var\{\Delta y1(\lambda_i)\}} = \frac{f0(\lambda_i)^2}{var\{y(\lambda_i)\}} \approx \frac{\langle y(\lambda_i)\rangle^2}{var\{y(\lambda_i)\}} = SNR(\lambda_i)^2 \quad (15)$$

where $\langle y(\lambda_i)\rangle$ is the average value of the lidar measurement which is assumed to be close to the initial estimate $f0(\lambda_i)$. Therefore, for each wavelength the weighting factors can be approximated by the SNR of the lidar measurement at that wavelength. As mentioned earlier, the SNRs are estimated based on the received signal pulse waveforms.

https://doi.org/10.5194/amt-2020-466
Preprint. Discussion started: 22 December 2020


Atmospheric Measurement Techniques Discussions

The XCO_2 and other parameters can now be solved using a standard linear least-squares fitting method with the loss function Eq. (13), Jacobian Eq. (14), and weighting factors Eq. (15). One method to carry out the least-squares fit is to use the pseudo inverse function, which gives a numerical solution to the parameter set, as

$$\boldsymbol{\Delta\widehat{S}} = \boldsymbol{G}\,\boldsymbol{\Delta Y1} \tag{16}$$

with $\boldsymbol{G}$ a $N_3 \times N_1$ matrix, which is often called gain matrix and can be computed from the pseudo inverse function $\boldsymbol{pinv}(\cdot)$ (Peters and Wilkinson, 1970), as

$$\boldsymbol{G} = \boldsymbol{pinv}[\boldsymbol{K}^T\boldsymbol{pinv}(\boldsymbol{W1})\boldsymbol{K}]\,\boldsymbol{K}^T\boldsymbol{pinv}(\boldsymbol{W1}). \tag{17}$$

The pseudo inverse matrix function can be found in Matlab and other software tools.

The covariance of the parameters can be obtained from Eq. (16), as

$$\mathbf{cov}\left(\boldsymbol{\Delta\widehat{S}}\right) = \boldsymbol{G}^T\,\mathbf{var}(\boldsymbol{\Delta Y1})\,\boldsymbol{G}. \tag{18}$$

with $\mathbf{var}(\boldsymbol{\Delta Y1})$ a diagonal matrix with the elements given by Eq. (15). The covariance matrix $\mathbf{cov}\left(\boldsymbol{\Delta\widehat{S}}\right)$ is in general not a diagonal matrix even though $\mathbf{var}(\boldsymbol{\Delta Y1})$ is a diagonal matrix.

The variances of the estimated parameters are given by the diagonal elements of $\mathbf{cov}\left(\boldsymbol{\Delta\widehat{S}}\right)$ as a measure of the goodness of the fit. However, variance is only one of the criteria of the XCO_2 retrieval. There can still be a bias in the estimated parameters if there is a mismatch between the measurements and the model.

5. Averaging Kernel

The averaging kernel is a function widely used in passive atmospheric sounding measurements. For these the vertical profile of CO_2 mixing ratio is retrieved and the averaging kernel is defined as (Rodgers, 2000),

$$\boldsymbol{A_p} = \frac{\partial \widehat{\boldsymbol{xco_2}}}{\partial \boldsymbol{xco_2}} = \boldsymbol{G_P K_p} \tag{19}$$

where $\widehat{\boldsymbol{xco_2}}$ and $\boldsymbol{xco_2}$ are the estimated and the actual CO_2 mixing ratio of the layers, respectively, $\boldsymbol{G_P}$ is the gain matrix and $\boldsymbol{K_p}$ is the Jacobian. The averaging kernel gives a measure of the sensitivity of the retrieved CO_2 mixing ratio to the actual one at the given altitude. However, the averaging kernel defined above cannot be used directly for our multi-wavelength IPDA lidar where only the column average XCO_2 is retrieved.

Here we define an averaging kernel specifically for the retrieval algorithm for our multi-wavelength IPDA lidar, as,

$$\boldsymbol{A_L} = \frac{\partial \widehat{XCO2}}{\partial \boldsymbol{xco_2}}. \tag{20}$$

where $\widehat{XCO2}$ is a scalar and equal to the estimated average column XCO_2. This new averaging kernel has N_2 elements, one per atmosphere layer. It gives a measure of the sensitivity of the retrieved average column XCO_2 to that of each layer. The retrieved XCO_2 can be expressed as the product of the retrieved scale factor and the *a priori* column average value, i.e., $\widehat{XCO2} = \widehat{\alpha co_2}\overline{XCO2}$. The averaging kernel can be written as

$$\boldsymbol{A_L} = \frac{\partial[\widehat{\alpha co_2}\overline{XCO2}]}{\partial \boldsymbol{xco_2}} = \left(\frac{\partial \widehat{\alpha co_2}}{\partial \boldsymbol{\Delta y1}}\right)\left[\overline{XCO2}\cdot\left(\frac{\partial \boldsymbol{\Delta y1}}{\partial \boldsymbol{xco_2}}\right)\right] = \boldsymbol{G_\alpha K_L}, \tag{21}$$

https://doi.org/10.5194/amt-2020-466
Preprint. Discussion started: 22 December 2020


Atmospheric Measurement Techniques Discussions

where $\boldsymbol{G_\alpha} = \partial \widehat{\alpha co}_2 / \partial \Delta \boldsymbol{y1}$ is the second row of the $\boldsymbol{G}$ matrix for calculating $\widehat{\alpha co}_2$ and $\boldsymbol{K_L}$ is an $N_1 \times N_2$ matrix and each term can be written according to Eqs. (4), (5) and (12), as

$$K_L(i,j) = \overline{XCO2} \cdot \frac{\partial \Delta y1(\lambda_i)}{xco2_j} = 2\overline{XCO2} \cdot N_{air}(H_j)\, \sigma_{CO2}(H_j, \lambda_i)\, \Delta H_j. \quad (22)$$

Therefore, each element of the averaging kernel becomes

$$A_L(H_j) \approx 2 \sum_{i=1}^{N_1} g_{2,j} \left[\overline{XCO2}\, N_{air}(H_j)\, \sigma_{CO2}(H_j, \lambda_i)\, \Delta H_j\right]. \quad (23)$$

The term in the bracket is the layered OD from the atmosphere model assuming uniform CO_2 mixing ratio $\overline{XCO2}$. Therefore, the averaging kernel is the sum of these layered ODs weighted by the corresponding terms of the $\boldsymbol{G}$ matrix.

6. Evaluation of the Retrieval Algorithm Using Airborne Lidar Data

The algorithm described here was used to retrieve XCO_2 from measurements of our 2017 airborne lidar campaign (Mao et al., 2019). The lidar and the airborne measurements have been described in detail in Abshire et al. (2018). Here we show an example of using the retrieval algorithm on a data set collected during one of the flights. We also show the retrieved XCO_2 at different altitudes in comparison to the in situ measurements made during two spiral-down maneuvers.

Figure 4 shows a segment of a Level-1data set from our 2017 airborne campaign. It shows 30 transmitted pulse waveforms and the corresponding received pulse waveforms averaged over 32 laser wavelength scans. The decrease (tilt) of laser pulse amplitudes over the pulse width interval is caused by the depletion of energy stored in the laser amplifier media, which does not affect the IPDA lidar measurements. The energies of the transmitted laser pulses fluctuate by a few percent, which is normalized out in the signal processing. The tails in the transmitted pulse waveforms shown in Fig. 4 (b) are caused by an artifact of the laser monitor detector, which is different from the one used in the receiver. The amplitudes and energies of the received laser pulse waveform plotted in Fig. 4 (c) clearly show the CO_2 absorption near the center of the wavelength scan. The XCO_2 retrieval is carried out at 1 Hz, during which the host aircraft typically travels about 200 m.

For the least-squares fit the weighting factor for each wavelength is the square of the SNR of the lidar detected signals at that wavelength. The SNRs are estimated from the received lidar signal as (Gagliardi and Karp, 1995)

$$SNR(\lambda_i) = \frac{\eta_d \langle n_s(\lambda_i)\rangle}{\sqrt{F_d\left[\eta_d\left(n_s(\lambda_i) + \left(1+\frac{\tau_s}{\tau_b}\right)\langle n_b\rangle\right) + \left(1+\frac{\tau_s}{\tau_b}\right)\langle n_d\rangle\right] + \left(1+\frac{\tau_s}{\tau_b}\right)\langle n_a\rangle^2/\langle G_d\rangle^2}}. \quad (24)$$

Here $\langle n_s(\lambda_i)\rangle$ is the average number of received signal photons per pulse at wavelength λ_i, $\langle G_d\rangle$ is the average gain of the avalanche photodiode (APD), η_d is the APD quantum efficiency, F_d is the APD gain excess noise factor, τ_s is the integration time for the signal pulse, τ_b is the integration time for the background and dark noise, $\langle n_b\rangle$ and $\langle n_d\rangle$ are the average number of background photons and detector dark counts integrated over the pulse interval, and $\langle n_a\rangle$ is the standard deviation of the preamplifier noise in terms of equivalent number of photoelectrons. The signal here refers to the number of detected signal photons, which is equal to the difference of the number of the detected photons minus the number of detected background photons.

https://doi.org/10.5194/amt-2020-466
Preprint. Discussion started: 22 December 2020

Atmospheric Measurement Techniques Discussions

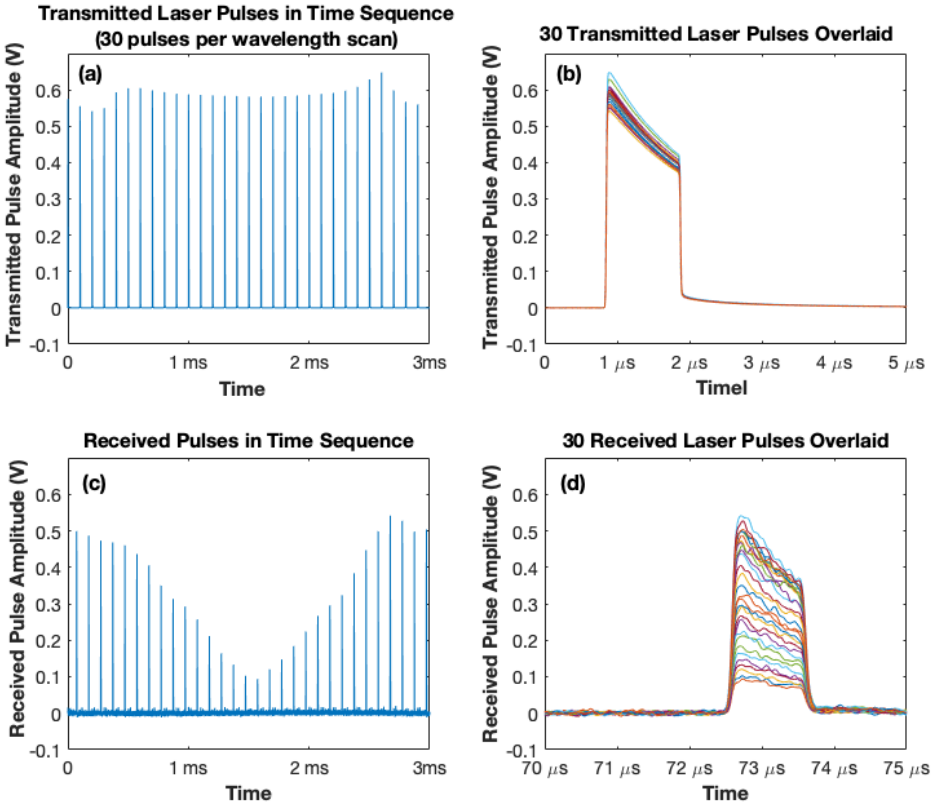

Figure 4. Sample pulse waveforms of the airborne CO_2 Sounder lidar taken during the flight of 7/21/2017 00:30:00 (UTC). (a) The 30 transmitted laser pulse waveforms in a wavelength scan averaged over 32 repeated scans; (b) overlay of transmitted pulse waveforms (c) the corresponding received laser pulse waveforms reflected from the ground surface showing the lidar sampled CO_2 absorption, and (d) an overlay of the received pulse waveforms.

For the XCO_2 retrieval, the average number of received signal photons are estimated from the received pulse waveform. This is obtained by first integrating the received pulse waveform from the detector in volts, dividing the result by the detector responsivity in volts/W, and the photon energy in Joules. The average number of background noise photons is estimated from the average surface reflectance, off-line atmosphere transmission, the nominal sun light irradiance on the surface, and the receiver optics model. All other parameter values in Eq. (24) are instrument related and can be found in Abshire et al. (2018).

https://doi.org/10.5194/amt-2020-466
Preprint. Discussion started: 22 December 2020

Atmospheric Measurement Techniques Discussions

Figure 5 shows the CO_2 absorption line shape sampled by the lidar along with that from the model assuming a constant *a priori* XCO_2 vertical profile of 400 parts per million (ppm). It also shows the placement of laser wavelengths across the CO_2 absorption line. One laser wavelength (the second from the left) was placed at a secondary peak due to water vapor. Three wavelengths were placed on the wings of the CO_2 absorption line. The rest were roughly equally spaced in OD along the absorption line. The residual differences between the measurements and the model after the least-squares fit is also plotted in Fig. 5.

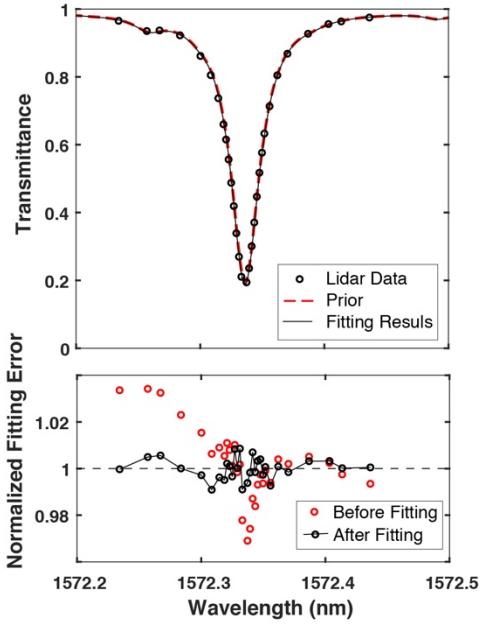

Figure 5. Top, an example of a CO_2 absorption line shape sampled by the airborne lidar (black circles) for 1-sec averaging time and the models before and after the fit (red and black lines). Bottom, differences (the residuals) between the lidar measurement and the models at the lidar wavelengths before (in red circles) and after (in black circles) the least-squares fit for the data set shown in Fig. 4.

The averaging kernel is calculated based on Eq. (22) for each fit of 1-second lidar measurement data. The averaging kernel and a 4^{th} order polynomial fit for the data shown above are plotted in Fig. 6.

Figure 7 shows the results of the retrieval using the algorithm described above from the airborne CO_2 Sounder lidar measurements made on July 21, 2017 starting at 00:30:00 for 820 seconds. The data consist of about 500 second segment measured at a nearly constant aircraft altitude followed by about 300 seconds in the spiral descent. The last part of the flight was near Edwards Air Force Base CA and the surface elevation was nearly constant for the last 500 seconds. The retrieved XCO_2 during this period was steady with a slow downward trend. The root-mean-squared (rms) variation of the retrieved XCO_2 from 2100 to 2300 seconds was 0.67 ppm, which includes both the fitting error and the actual XCO_2 variation along the flight path. By comparison, the estimated standard deviation from the covariance matrix was about 0.35 ppm (Fig. 7).

https://doi.org/10.5194/amt-2020-466
Preprint. Discussion started: 22 December 2020

Atmospheric Measurement Techniques Discussions

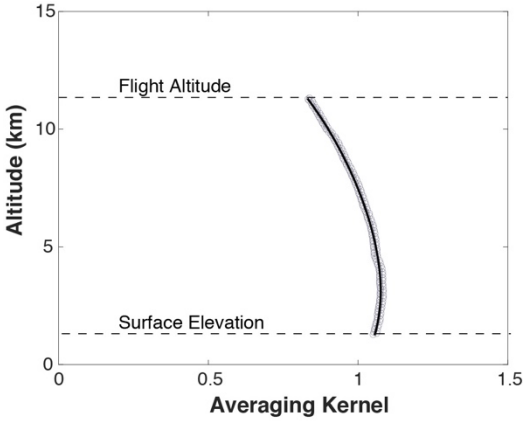

335

Figure 6. The averaging kernel from the retrieved data (open circles) and the 4th order polynomial fit with altitude (solid black curve) from the measurement data shown in Fig. 5.

Figure 8 shows the retrieved XCO_2 compared to the in situ measurements as the airplane flew in a spiral-down path
340 from 12 km to 4 km over Edwards Air Force Base for the flight on July 21, 2017 and the final science flight on August 8, 2017. The in situ profile was measured by an updated version of the AVOCET gas analyzer on board the airplane (Vay et al., 2011). The in situ XCO_2 at the airplane altitude is obtained by integrating the CO_2 profile from the in situ measurements weighted by the same averaging kernel. The XCO_2 retrieved from the lidar measurements agrees with that from the in situ measurements at all airplane altitudes above 4 km. Below 4 km, the laser beam no longer completely overlaps the receiver
345 field of view and the total CO_2 absorption (line depth) becomes too low to be reliably measured.

https://doi.org/10.5194/amt-2020-466
Preprint. Discussion started: 22 December 2020

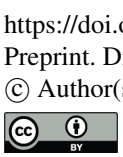

Atmospheric Measurement Techniques Discussions

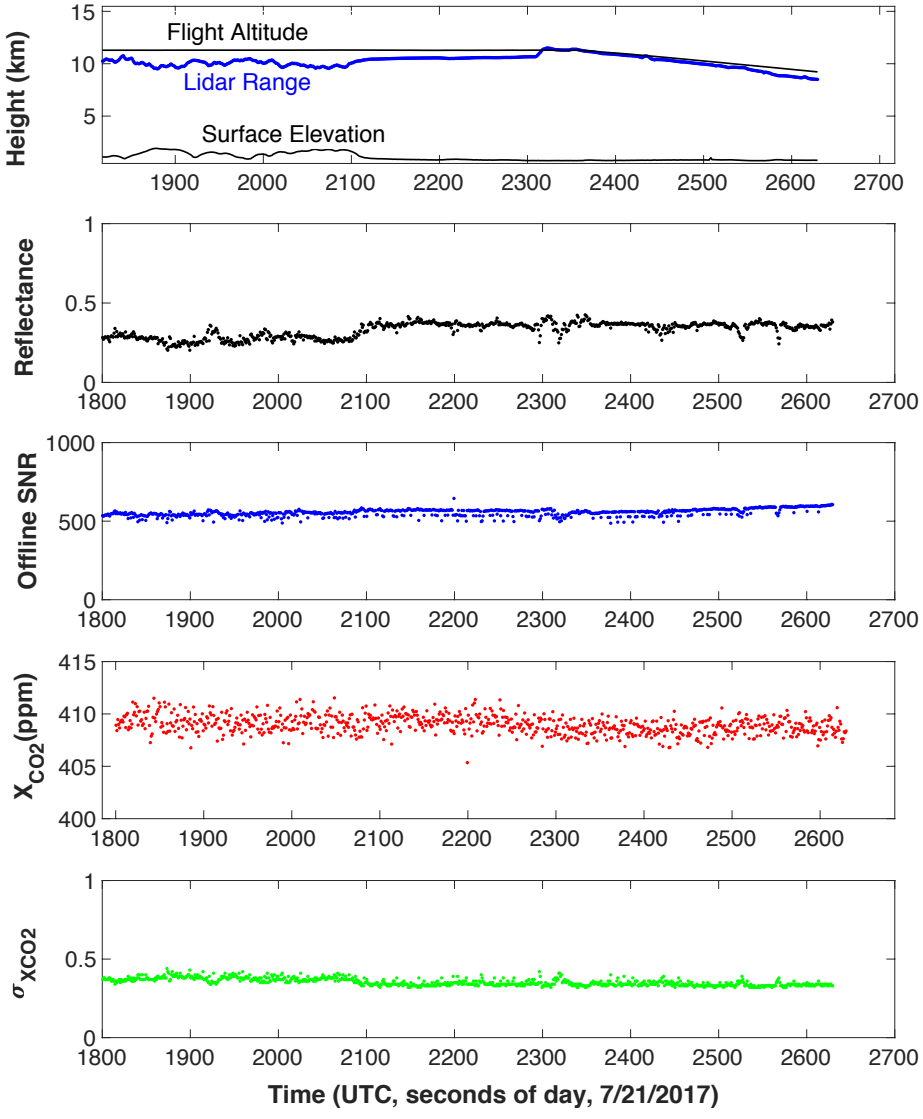

Figure 7. The results of the retrieval sequence from the airborne CO_2 Sounder lidar data starting at 7/21/2020 00:30:00 UTC for 820 seconds over Edwards Air Force Base in California. These are all based on 1-second receiver integration time. They are, from top down, (a) the aircraft altitude, the lidar range from the laser pulse time of flight, and surface elevation from the on board GPS receiver, the radar altimeter, and the digital elevation map; (b) the retrieved surface reflectance times the two-way off-line atmospheric transmission; (c) off-line SNR calculated from Eq. (24); (d) the retrieved XCO_2; and (e) standard deviation of the retrieved XCO_2 from the covariance matrix.

https://doi.org/10.5194/amt-2020-466
Preprint. Discussion started: 22 December 2020

Atmospheric Measurement Techniques Discussions

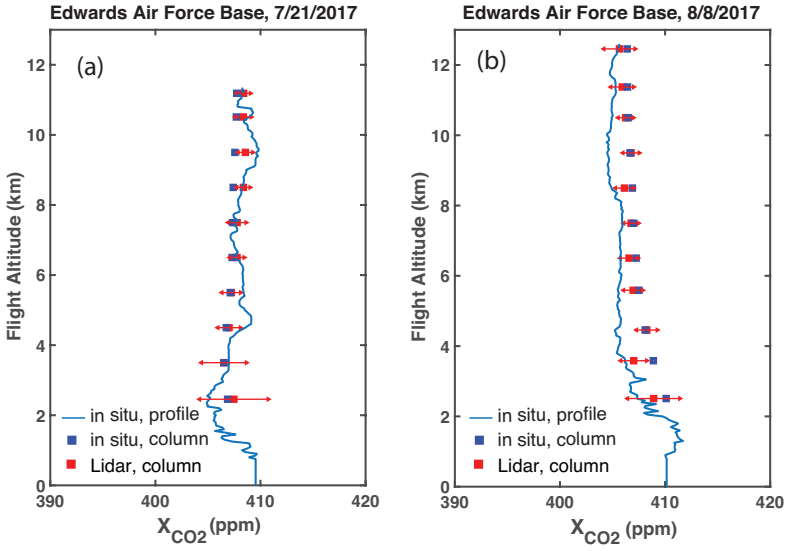

Figure 8. The column XCO_2 retrieved from the lidar measurements (red squares) compared to that from the in situ measurements (blue squares) during the spiral-downs on (a) July 21, 2017 and (b) August 8, 2017. The error bars on the red squares represent mean and the standard deviation of the lidar measurement results binned into 1-km layers. The blue squares are the column integrated readings of the AVOCET gas analyzer from the altitude plotted to the surface. For the spiral-down comparisons, the median differences (biases) between the retrieved lidar and column *in situ* measurements are 0.72 ppm for July 21 and 0.16 ppm for August 8, 2017.

7. Discussion

7.1 Biases in the Retrieved XCO2

The least-squares-fit method minimizes the sum of squared errors but does not guarantee minimum biases in the estimated parameters. The variances of the solutions approach zero as the SNR increases, as shown in Eq. (18). However, a mismatch between the CO_2 absorption line shape derived from the model and the actual line shape can cause biases in the retrieved results. Therefore, it is important to model the atmosphere accurately and avoid systematic errors.

7.2. Choice of Laser Wavelengths

The choice of the laser wavelengths is a tradeoff among several factors. The total number of laser wavelengths has to be greater than the number of parameters to be solved from the lidar measurements. However, the total average laser output power is fixed. Using fewer wavelength samples improves the SNR for each sample, but provides fewer constraint to the fit. More wavelength samples lower the SNR at each wavelength, but allows solving for more parameters and help to reduce the bias in

https://doi.org/10.5194/amt-2020-466
Preprint. Discussion started: 22 December 2020


Atmospheric Measurement Techniques Discussions

the XCO_2 retrieval. There is also an advantage to select the laser wavelengths to be symmetrically distributed about the line center since the effect of the nonuniformity in the receiver's spectral response may cancel out (Chen et al., 2019).

The airborne CO_2 Sounder lidar mostly used 30 wavelengths with four off-line, four about the center of the peak absorption up to OD=1.2, one on the water vapor peak absorption, and the rest approximately uniformly distributed in OD (Abshire et al, 2018). This choice of the laser wavelengths produced measurement precisions < 1 ppm and biases < 1 ppm. Abshire et al., (2018) also report airborne measurement made using 15 laser wavelengths that showed no apparent difference in the XCO_2 measurements to those using 30 wavelengths.

7.3. Number of Parameters to Retrieve

It is possible to use the least-squares fit to solve for more parameters of the CO_2 line and lidar instrument, as long as the number of parameters to retrieve is less than the degrees of freedom of the lidar measurements. However, solving for more parameters, especially when they are correlated, increases the variance in the retrieved values, which limits the benefit.

One example is to divide the atmosphere into a few layers, each with its own line shape function and scale factor, to obtain some information about the vertical distribution of XCO_2. However, the results from the least-squares fit for the XCO_2 for the layers are correlated and the errors from the fits are usually too large to be useful (Chen et al., 2014). A singular value decomposition (SVD) method also has been used to extract a few more parameters about the line shape without the need for an *a priori* vertical XCO_2 profile (Ramanathan et al., 2018). The SVD method can retrieve the certain characteristics of the line shape and provide certain information about the vertical distribution of XCO_2

Conclusion

An algorithm to retrieve XCO_2 has been developed for measurements from a pulsed multi-wavelength integrated path differential absorption (IPDA) lidar. The retrieval algorithm uses a least-squares fit of the line shape function derived from a multi-layer atmosphere radiative transfer model based on meteorological data to the line shape sampled by the lidar measurements. In addition to XCO_2, the algorithm simultaneously solves for the product of the surface reflectance and the off-line atmosphere transmission, Doppler shift of the received laser signals, a secondary water vapor mixing ratio (if present), and a linear trend of the lidar receiver non-uniformity in its spectral response. Since it can accurately retrieve XCO2 in the presence of these conditions, this approach provides a more robust measurement of XCO_2 compared to IPDA lidar that use only on-line and off-line wavelengths. The retrieval algorithm has been used successfully in the data processing of the NASA Goddard's multi-wavelength pulsed IPDA lidar from its 2016 and 2017 airborne campaigns. The algorithm may also be used for retrievals for multi-wavelength lidar that target other atmospheric gases, such as CH_4.

https://doi.org/10.5194/amt-2020-466
Preprint. Discussion started: 22 December 2020

Atmospheric Measurement Techniques Discussions

References

Abshire, J. B., Riris,H., Allan, G. R., Weaver, C., Mao, J., Sun, X., Hasselbrack, W. E., Kawa, S. R., and Biraud, S.: Pulsed airborne lidar measurements of atmospheric CO2 column absorption, Tellus B, 62(5), 770-783, 2010.

Abshire, J. B., Riris, H., Weaver, C., Mao, J., Allan, G., Hasselbrack, W., and Browell, E. V.: Airborne measurements of CO2 column absorption and range using a pulsed direct-detection integrated path differential absorption lidar, Appl. Optics, 52, 4446–4461, 2013.

Abshire, J. B., Ramanathan, A., Riris, H., Mao, J., Allan, G. R., Hasselbrack, W. E., Weaver, C. J., and Browell, E.V.: Airborne measurements of CO2 column concentration and range using a pulsed direct-detection IPDA lidar, Remote Sens., 6, 443–469, 2014.

Abshire, J. B., Ramanathan, A., Riris, H., Allan, G. R., Sun, X., Hasselbrack, W. E., Mao, J., Wu, S., Chen, J., Numata, K., Kawa, S. R., Ying, M., Yang, M., and DiGangi, J.: Airborne measurements of CO_2 column concentrations made with a pulsed IPDA lidar using multiple-wavelength-locked laser and HgCdTe APD detector, Atmos. Meas. Tech., 11, 2001-2025, 2018.

Amediek, A., Ehret, G., Fix, A., Wirth, M., Büdenbender, C., Quatrevalet, M., Kiemle, C., and Gerbig, C.: CHARM-F: A new airborne integrated-path differential-absorption lidar for carbon dioxide and methane observations: measurement performance and quantification of strong point source emissions, Appl. Optics, 56, 5182–5197, 2017.

Allan, G. R., Sun, X., Abshire, J. B., Riris, H., Hasslbrack, W. E., Kawa, S. R. Numata, K., Mao, J. and Chen, J.: Atmospheric backscattering profiles from the 2017 ASCENDS/ABoVE airborne campaign measured by the CO_2 Sounder lidar, 2019 Fall AGU Annual Meeting, San Francisco, CA, Dec. 9-13, 2019, Paper A51M-2726.

Bevington, P. R.: Data Reduction and Error Analysis for the Physical Science, McGraw-Hill, New York, 1969, Ch. 6.

Chen, J. R., Numata, K., and Wu, S. T.: Error reduction in retrieval of atmospheric species from symmetrically measured lidar sounding absorption spectra, Opt. Express, 22, 26055-26075, 2014.

Chen, J. R., Numata, K., and Wu, S. T.: Error analysis for lidar retrievals of atmospheric species from absorption spectra, Opt. Express, 27, 36487-36504, 2019.

Clough, S. A., Iacono, M. J. and Moncet, J.: Line-by-line calculations of atmospheric fluxes and cooling rates: Application to water vapor, J. Geophys. Res. Atmos. 97, 15,761-715,785, 1992.

Clough, S. A. & Iacono, M. J.: Line-by-line calculation of atmospheric fluxes and cooling rates 2. Application to carbon dioxide, methane, nitrous oxide and the halocarbons, J. Geophys. Res. Atmos. 100, 16,519-516,535, 1995.

Crisp, D., Pollock, H. R., Rosenberg, R., Chapsky, L., Lee, R. A. M., Oyafuso, F. A., Frankenberg, C., O'Dell, C. W., Bruegge, C. J., Doran, G. B., Eldering, A., Fisher, B. M., Fu, D., Gunson, M R., Mandrake, L., Osterman, G. B., Schwandner, F. M., Sun, K., Taylor, T. E., Wennberg, P. O., and Wunch, D.: The on-orbit performance of the Orbiting Carbon Observatory-2 (OCO-2) instrument and its radiometrically calibrated products, Atmos. Meas. Tech. 10, 59-81, 2017.

https://doi.org/10.5194/amt-2020-466
Preprint. Discussion started: 22 December 2020


Atmospheric Measurement Techniques Discussions

435 Dobler, J., Harrison, F., Browell, E., Lin, B., McGregor, D., Kooi, S., Choi, Y., and Ismail, S.: Atmospheric CO2 column measurements with an airborne intensity-modulated continuous wave 1.57 um fiber laser lidar, Appl. Optics, 52, 2874–2892, 2013.

Eldering, A., O'Dell, C. W., Wennberg, P., Crisp, O. D., Gunson, M. R., Viatte, C., et al.: The Orbiting Carbon Observatory-2: first 18 months of science data products, Atmos. Meas. Tech., 10, 549–563, 2017.

440 Eldering, A., Taylor, T. E., O'Dell, C. W., and Pavlick, R.: The OCO-3 mission: measurement objectives and expected performance based on 1 year of simulated data, Atmos. Meas. Tech., 12, 2341–2370, 2019.

Gagliardi, R. M. and Karp, S.: Optical Communications, 2nd ed, John Wiley and Sons, 1995.

Han, G., Shi, T., Ma, X., Xu, H., Zhang, M., Liu, Q., and Gong, Wei, G.: Obtaining gradients of XCO2 in atmosphere using the constrained linear least-squares technique and multi-wavelength IPDA LiDAR, Remote Sens., 12, 2395, 2020.

445 Jacob, J. C., Menzies, R. T., and Spiers, G. D.: Data processing and analysis approach to retrieve carbon dioxide weighted-column mixing ratio and 2-μm reflectance with an airborne laser absorption spectrometer, IEEE Trans. Geosci. Remote Sens., 57(2), 958-971, 2019.

Kawa, S. R., Abshire, J. B., Sun, X., Mao, J., and Ramanathan, A.: Updated performance simulations for a space-based CO_2 lidar mission, 12th International Workshop on Greenhouse Gas Measurements from Space (IWGGMS-12), Jun. 7-9, 2016,

450 Kyoto, Japan, Paper 48, https://www.nies.go.jp/soc/events/iwggms12/pdf/Session_10/48_Stephan_Kawa.pdf.

Kawa, S. R., Abshire, J. B., Baker, D. F., Browell, E. V., Crisp, D., Crowell, S. M. R., Hyon, J. J., Jacob, J. C., Jucks, K. W., Lin, B., et al.: Active Sensing of CO2 Emissions over Nights, Days, and Seasons (ASCENDS): Final Report of the ASCENDS Ad Hoc Science Definition Team, Document ID: 20190000855, NASA/TP–2018-219034, GSFC-E-DAA-TN64573, 2018.

455 Kuze, A., Suto, H., Shiomi, K., Kawakami, S., Tanaka, M., Ueda, Y., Deguchi, A., Yoshida, J., Yamamato, Y., Kataoka, F., Taylor, T. E., and Buijs, H. L., Update on GOSAT TANSO-FTS performance, operations, and data products after more than 6 years in space, Atmos. Meas. Tech., 9, 2445–2461, 2016.

Mao, J., Ramanathan, A., Abshire, J. B., Kawa, S. R., Riris, H., Allan, G. R., Hasselbrack, W. E., Sun, X., Chen, J., and Numata, K.: Atmospheric CO_2 concentration measurements to cloud tops from airborne lidar measurement during

460 ASCENDS science campaigns, Atmos. Meas. Tech., 11, 127-140, 2018.

Mao, J., Abshire, J. B., Kawa, S. R., Riris, H., Allan, G. R., Hasselbrack, W. E., Numata, K., Chen, J., Sun, X., Nicely, J. M., DiGangi, P. J., and Choi, Y.: Airborne demonstration of atmospheric cO2 concentration measurements with a pulsed multi-wavelength IPDA lidar, 15th International Workshop on Greenhouse Gas Measurements from Space (IWGGMS), Jun. 3-5, 2019, Sapporo, Japan, Paper 5-5, www.nies.go.jp/soc/doc/Oral_Presentations/Session5-6/5-

465 5_iw15op_Jianping_Mao.pdf.

Menzies, R. T., Spiers, G. D., and Jacob, J.: Airborne laser absorption spectrometer measurements of atmospheric CO_2 column mole fractions: source and sink detection and environmental impacts on retrievals, J. Atmos. Ocean Technol., 31, 404-421, 2014.

https://doi.org/10.5194/amt-2020-466
Preprint. Discussion started: 22 December 2020


Atmospheric Measurement Techniques Discussions

McManamon, P. LiDAR, Technologies and Systems, SPIE Press, Bellingham, 2019, Ch. 3.

Peters, G. and Wilkinson, J. H.: The least squares problem and pseudo-Inverses, The Computer Journal, 13, 309-316, 1970, https://doi.org/10.1093/comjnl/13.3.309.

Numata, K., Chen, J. R., and Wu, S. T.: Precision and fast wavelength tuning of a dynamically phase-locked widely-tunable laser, Opt. Express, 20, 14234-14243, 2012.

Ramanathan, A., Mao, J., Allan, G. R., Riris, H., Weaver, C. J., Hasselbrack, W. E., Browell, E. V., and Abshire, J. B.: Spectroscopic measurements of a CO2 absorption line in an open vertical path using an airborne lidar, Appl. Phys. Lett., 103, 214102 (2013).

Ramanathan, A. K., Mao, J., Abshire, J., and Allan, G. R.: Remote sensing measurements of the CO_2 mixing ratio in the planetary boundary layer using cloud slicing with airborne lidar, Geophys. Res. Lett., 42, 2055-2062, 2015.

Ramanathan, A. K., Nguyen, H. M., Sun, X., Mao, J., Abshire, J. B., Hobbs, J. M., and Braverman, A. J.: A singular value decomposition framework for bias-free retrievals with vertical distribution information from column greenhouse gas absorption spectroscopy measurements, Atmos. Meas. Tech., 11, 4909-4928, 2018.

Refaat, T. F., Singh, U. N., Yu, J., Petros, M., and Ismail, S.: Double-pulse 2-μm integrated path differential absorption lidar airborne validation for atmospheric carbon dioxide measurement, Appl. Optics, 55, 4232-4246, 2016.

Refaat, T. F., Petros M., Singh, U. N., Antill, C. W., and Remus, Jr., R. G.: High-precision and high-accuracy column dry-air mixing ratio measurement of carbon dioxide using pulsed 2-μm IPDA lidar, IEEE Trans. Geosci. Remote Sens., 58(8), 5804-5819, 2020

Rienecker, M.M., Suarez, M.J., Gelaro, R.; Todling, R., Bacmeister, J., Liu, E.; Bosilovich, M.G., Shubert, S.D., Takacs, L., Kim, G.-K., et al.: MERRA: NASA's modern-era retrospective analysis for research and applications. J. Clim., 24, 3624–3648, 2011.

Rodgers, C. D.: Inverse Methods for Atmospheric Sounding*, Theory and Practice*, World of Scientific Publishing, Singapore, 2000.

Rothman, L., et al.: The HITRAN 2008 molecular spectroscopic database, J. Quant. Spectros. Radiat. Transfer, 110(9), 533–572, 2009.

Sellers, P. J., Schimel, D. S., Moore III, B., Liu, J., and Eldering, A.: Observing carbon cycle–climate feedbacks from space. Proceedings of the National Academy of Science of the United States of America, 115(31), 7860–7868, 2018.

Spiers, G., Menzies, R., Jacob, J., Christensen, L., Phillips, M., Choi, Y., and Browell, E.: Atmospheric CO2 measurements with a 2 μm airborne laser absorption spectrometer employing coherent detection, Appl. Optics, 50, 2098–2111, 2011.

Vay, S. A., Choi, Y., Vadrevu, K. P., Blake, D. R., Tyler, S. C., W., Woo, J.-H., Weinheimer, A. J., Burkhart, J. F., Stohl, A., and Wennberg, P. O., Wisthaler, A., Hecobian, A., Kondo, Y., Diskin, G. S., and Sachse, G.: Patterns of CO2 and radiocarbon across high northern latitudes during International Polar Year 2008, J. Geophys. Res.-Atmos., 116, D14301, 2011.

Zhu, Y., Liu, J., Chen, X., Zhu, D. B., and Chen, W.: Sensitivity analysis and correction algorithms for atmospheric CO_2 measurements with 1.57-μm airborne double-pulse IPDA LIDAR, Opt. Express, 27, 32679-32699, 2019.

https://doi.org/10.5194/amt-2020-466
Preprint. Discussion started: 22 December 2020

Zhu, Y., Yang, J., Chen, X., Zhu, X., Zhang, J., Li, S., Sun, Y., Hou, X., Bi, D., Bu, L., Zhang, Y., Liu, J., and Chen, W.:
505 Airborne validation experiment of 1.57-μm double-pulse IPDA lidar for atmospheric carbon dioxide measurement, Remote Sens., 12, 1999, 2020.